A numerical model for the calculation of electromagnetic interference from power lines on nonparallel underground pipelines

A numerical model for the calculation of electromagnetic interference from power lines on nonparallel underground pipelines

Arturo Popoli[a,*], Andrea Cristofolini[a], Leonardo Sandrolini[a]

[a]*Department of Electrical, Electronic and Information Engineering, University of Bologna, Bologna, 40136, Italy*

Abstract

This work proposes a numerical methodology for the calculation of currents and voltages induced on underground pipelines by nearby overhead power lines. A previously developed quasi-3D methodology is extended, allowing the investigation of nonparallel routings of the pipelines with respect to the power lines. The proposed technique is based on a discretization of the pipeline path into several segments parallel to the power line. The section of the corridor corresponding to each pipeline segment is regarded as an electrical multi-port component, whose electrical parameters are extracted via finite element 2D analysis. Then, the obtained components are integrated into a network embodying the physical characteristics of the whole corridor. In this way, the circuital analysis is used to extend the capabilities of a standard two-dimensional field analysis. The proposed methodology is employed to simulate a pipeline running parallel to a power line for a distance of 12 km. Afterwards, several nonparallel configurations - consisting of crossings between a pipeline and a power line - are assessed. The physical consequences of the crossing are discussed and a convergence study is performed to investigate the optimal pipeline subdivision procedure to be adopted for a set of different crossing angles.

Keywords: Electromagnetic Compatibility, Electromagnetic Coupling, Finite Element Analysis, Pipelines, Equivalent Circuit.

1. Introduction

The problem of assessing the electromagnetic interference induced by AC power lines on buried metallic pipelines has been considered by a number of authors. The studies are motivated by the fact that the electromotive forces generated in a pipeline may produce corrosion effects and may endanger people that come in contact with this structure. However, while safety and technical reasons demand accurate estimations of the induced interference levels, this task still represents a scientific challenge; indeed, a metallic pipeline buried in soil constitutes an earth-return electrical circuit, whose physical characteristics

*Corresponding author
Email address: arturo.popoli@unibo.it (Arturo Popoli)

depend, among other parameters, on the path taken by the current flowing through the soil [1]. The coupling between power lines and pipelines is usually represented by means of current controlled voltage sources, acting as forcing terms for the lossy transmission line models used to model the metallic pipelines [2, 3]. The scientific papers and technical standards based on these analytical methodologies generally employ some kind of approximation of Carson's expressions to estimate the mutual impedance between the considered earth return structures [4, 5]; in order to allow the use of these analytical expressions, a "weak coupling" assumption is adopted; depending on the complexity of the considered physical configuration, this can lead to neglecting important physical contributions as discussed in [6]. The use of circuital approaches combined with 2D finite differences or finite element analysis has then been introduced in order to overcome these limitations and allow the analysis of complex domains, such as those involving multilayered soils [7] or including a large number of conductors [8–10]. These approaches are based on building an equivalent lumped parameter network built using parameters calculated with the FEM method, such as the self- and mutual impedances of the conductors [11–13]. The obvious extension of these methodologies is represented by performing 3D simulations of interference problems. Full 3D FEM models have been indeed employed to assess the local current density distributions at the interface between a pipeline and a lossy soil [14, 15], but focusing only on a limited region surrounding a specific point of the pipeline. An interesting combination of a 1D FEM and 3D BEM can be found in [16], where a 1D finite element methodology is employed for the pipeline internal and the 3D BEM for the external problem. Nevertheless, the choice of a Boundary Element Methodology requires to rely on complex image theory for the evaluation of the soil's physical contributions, differently from FEM analysis in which the whole soil is discretized. To the authors' best knowledge, there are no examples of full 3D FEM models employed for the assessment of an entire right-of-way in the existing literature. The reason for this is the sheer amount of memory and overall computational burden that would be required to perform a 3D simulation including a power line, a pipeline and the surrounding soil. As an example, a typical 2D triangular mesh employed for this kind of simulations consists of a circular section with a radius of several hundreds of metres to include an adequately large portion of air and soil around the considered metallic conductors. The geometrical sizes of the elements range from tens of meters (outer edge of the domain) to sub-millimetric lengths (pipeline, power line conductors), in order to adequately account for the skin effect phenomenon. A reasonable number of nodes for a 2D mesh with these characteristic can be 40.000, giving roughly 80.000 triangular elements. In order to create a 3D mesh of a corridor, it would be required to "extrude" the described section for distances that typically span over several kilometres. Let now assume to employ a coarse subdivision of the axial direction, such as 1 m for each 3D brick element. Given that each brick is composed of 3 tetrahedral elements, and assuming a corridor length of 10 km, the resulting 3D mesh would require $80.000 \cdot 10.000 \cdot 3 = 2.4 \cdot 10^9$ tetrahedrons. It is also useful to point out that the provided rough estimation does not account for the necessity of a finer discretization of any eventual earthing system of the power line or the pipeline, making $2.4 \cdot 10^9$ tetrahedrons a rather optimistic estimate. The quasi-3D approach developed in [17] consists of using FEM simulations to incorporate the physical dependencies among the conductors of a given corridor section into an equivalent multiport electrical component. This can be included in an equivalent network, which allows the physical effects produced by what lies upstream and downstream of each section of

the routing to be taken into account, such as the power sources and loads of the power line, or the imperfect coatings and groundings of the pipeline. It is worth highlighting that - for each section of the considered corridor - the obtained results are the same that would be yielded by a 2D FEM simulation with the appropriate constraints. In [17], the methodology was applied to a case of parallelism between the overhead power line and the victim pipeline. In this paper, the methodology is extended to configurations where the pipeline presents a more complex routing with respect to the power line, possibly including crossings. This is achieved by subdividing the geometry into several sections, each regarded as a multi-port electrical component; the equivalent lumped parameter network representing the overall interference configuration results then from the cascade of individual multi-port electrical components. Section 2 provides details on the implementation of the proposed methodology. Afterwards, in Section 3 a 12 km long corridor is analysed assuming both a parallel and a nonparallel routing of the pipeline. A discussion on the dependency of the results from the pipeline discretization process is also provided in Section 3.2.

2. Numerical Model Description

As anticipated, the quasi-3D methodology described in this paper uses a circuital method to enforce some physical constraints on the physical information that can be inferred from a finite element analysis of a 2D geometry. For this reason, a dedicated finite element solver is here described, followed by the details regarding the equivalent circuit solution.

2.1. FEM formulation

For the considered problem, the aim of the finite element analysis is to compute the spatial distribution of the magnetic vector potential produced by the meshed conductors. In order to reduce the complexity of both the discretization and calculation processes, the following physical assumptions are assumed to be acceptable:

- linear and isotropic electrical properties of the materials (e.g., if a ferromagnetic medium is present, the nonlinearity of its magnetization curve is neglected);
- quasi-magnetostatic problem, i.e., the contribution of the displacement current $\partial D/\partial t$ is negligible with respect to the conduction current density J in the Ampére-Maxwell law;
- steady-state regime, which allows representing the electromagnetic fields as complex phasors;
- infinite length of the conductors.

The last assumption is justified if the distance between the pipeline and the power line is short compared to the extension of the corridor under analysis. This is true for most of the practical cases, and it allows considering the current density $\vec{J}$ and the magnetic vector potential $\vec{A}$ as directed along a preferential direction, i.e., if the power line is directed along the z-axis, $\vec{J} = J_z(x, y, t)\hat{k}$, $\vec{A} = A_z(x, y, t)\hat{k}$.

This assumption can be extended to the case of a pipeline oblique with respect to the power line, which can be thought as a sequence of small segments parallel to the power line. Let's consider a given frame of reference Ω and a straight power line, directed along the z direction of Ω. The assumption of infinite length of the conductors means the considered current densities $\vec{J}(x,y,z)$ are directed only along the z direction, and that $\vec{J}$ is constant along z. Therefore, $\vec{J}(x,y,z) = J_z(x,y)\hat{k}$, and as a consequence the magnetic field components exist only in the $x-y$ plane, $\vec{B} = B_x(x,y)\hat{i} + B_y(x,y)\hat{j}$. If another infinite conductor (such as a pipeline) is oblique with respect to the power line and carries a current density $\vec{J'}$ the magnetic field $\vec{B'}$ produced by the $\vec{J'}$ current will inevitably have a non-null component in the z direction of the power line frame of reference Ω, hence $\vec{B'} = {B'}_x(x,y,z)\hat{i} + {B'}_y(x,y,z)\hat{j} + {B'}_z(x,y,z)\hat{k}$. However, the $\hat{k}$ component of $\vec{B'}$ will necessarily be parallel to the power line, and hence (for the Faraday Law) will not produce any relevant induction effect. For this reason, at each given point of the pipeline, only the $\hat{k}$ component of the current density is relevant, and the pipeline can (locally) be represented with an infinite straight conductor parallel to the power line carrying a current density $\vec{J} = J_z(x,y)\hat{k}$.

Thanks to the aforementioned assumptions, the parabolic partial differential equation describing the diffusion of the magnetic vector potential can be rewritten as the following stationary complex expression:

$$-\nabla \cdot \left(\frac{1}{\mu}\nabla \underline{A_z}\right) = \underline{J_{0,z}} - j\omega\sigma\underline{A_z}. \tag{1}$$

In (1), $\underline{A_z}$ is the phasor representing the unknown sinusoidal vector potential, whereas the $\underline{J_{0,z}}$ term is the phasor accounting for the impressed current densities due to externally applied fields along the z direction (such as the three-phase power line source). Equation (1) can be discretized by means of a finite element method [18], defining a piecewise polynomial approximation $\underline{\tilde{A}_z}$ of the unknown function on a triangulation of a generic $x-y$ section Ω of the considered system. Defining a set of shape functions $\{N\}$ as a basis of the piecewise polynomial approximation, one may write $\underline{\tilde{A}_z} = \{N\}^T\{\underline{A_z}\}$, where $\{\underline{A_z}\}$ is an array whose elements are the nodal approximated values of $\underline{A_z}$. Following a Galerkin approach, a weak formulation [18] of the weighted residuals can be written as:

$$\int_\Omega \nabla N_k \cdot \left(\frac{1}{\mu}\nabla \underline{\tilde{A}_z}\right) \mathrm{d}S + j\omega \int_\Omega N_k \sigma \underline{\tilde{A}_z} \mathrm{d}S = \int_\Omega N_k \underline{J_{0,z}} \mathrm{d}S - \oint_{\partial\Omega} N_k \frac{1}{\mu}\frac{\partial \underline{\tilde{A}_z}}{\partial n}\mathrm{d}l, \tag{2}$$

where $\partial\Omega$ is the boundary of the plane calculation domain Ω. Applying (2) for all the mesh nodes, a complex linear system is obtained:

$$[\boldsymbol{K}]\{\boldsymbol{A}_z\} = \{\boldsymbol{f}\}, \tag{3}$$

which, once solved, yields the values of $\underline{A_z}$ on the mesh. In (3), the right hand side takes into account the imposed current densities $\underline{J_{0,z}}$ and the boundary conditions applied to $\partial\Omega$, and thus the relationship between the forcing terms and the effects, described by the vector potential distribution, that they produce on the considered section. However, it

should be noted that the forcing terms $\underline{J_{0,z}}$ are related to the longitudinal electric fields, and are generally not known *a priori*, since they depend on the behaviour of the whole system. Hence, in order to solve the problem on a given section, one must provide a way to appropriately couple the section taken into consideration and the rest of the corridor.

2.2. Equivalent circuit

Considering now a corridor with a generic routing, this can be approximated by a sequence of segments of finite longitudinal length. For each of these segments, the proposed method uses the finite element analysis just described to derive a linear relation between the forcing terms and the electric currents in each conductor. Since the current density, according to the symbolic representation used, can be expressed as:

$$\underline{J_z} = \underline{J_{0,z}} - j\omega\sigma\underline{A_z}, \tag{4}$$

the electric current $\underline{I_h}$ in a generic conductor h can be obtained by integrating $\underline{J_z}$ over its area S_h on the $x-y$ domain Ω, as:

$$\underline{I_h} = \int_{S_h} \underline{J_z}\mathrm{d}S = \int_{S_h} \underline{J_{0,z}}\mathrm{d}S - j\omega \int_{S_h} \sigma\underline{A_z}\mathrm{d}S. \tag{5}$$

Then, the linear relation between the array $\{\underline{I}\}$ constituted by the electric currents $\underline{I_1}, \underline{I_2}, \ldots, \underline{I_n}$ in each conductor, and the forcing term array $\{\underline{J_{z,0}}\}$, whose entries are the impressed current densities $\underline{J_{z,0,1}}$, $\underline{J_{z,0,2}}$, $\ldots$, $\underline{J_{z,0,n}}$ on the conductors can be written as:

$$\{\underline{I}\} = [\underline{M}]\{\underline{J_{z,0}}\}. \tag{6}$$

Equation (6) can be considered as a definition of the characteristic matrix $[\underline{M}]$. Assuming a system where there are n conductors (including OGWs and the soil), $[\underline{M}]$ is a rank n complex square matrix whose the generic entry $m_{h,k}$ is the current $\underline{I_h}$ flowing through the hth conductor when a unit current density $\underline{J_{0,z,k}}$ is enforced on the kth one. The characteristic matrix is then populated by running n FEM simulations, in each of which all the entries in $\underline{J_{z,0}}$ are set to zero, except $\underline{J_{0,z,k}}$ which assumes unit value. The entries in kth column of $[\underline{M}]$ are found by calculating the current on the conductors according to (5).

The characteristic matrix only depends on the geometry of the considered section (i.e. conductors dimensions and their relative positions) and on the electric and magnetic properties of the materials (i.e. electric conductivity and magnetic permeability). Considering now a generic segment of a corridor with a longitudinal length L, in the kth conductor the $\underline{J_{z,0,k}}$ impressed current is related to the voltage $\underline{V_k}$ applied to the conductor along the length L by:

$$\underline{J_{z,0,k}} = \frac{\sigma_k}{L}\underline{V_k}. \tag{7}$$

Thus, (6) can be regarded as a constitutive relation of a n-port circuit element. The whole corridor can then be modelled by an electric network like the one shown in Fig. 1 by way of example, where each corridor segment is represented by means of its characteristic matrix which is found via FEM simulation. It is also possible to take into account transversal resistive couplings between the various conductors (such as the currents between the pipeline and the ground due to imperfect insulation) by introducing into the network appropriate admittances ($\underline{Y}$ in Fig. 1). Network analysis is performed utilising a Tableau analysis, as detailed in [17].

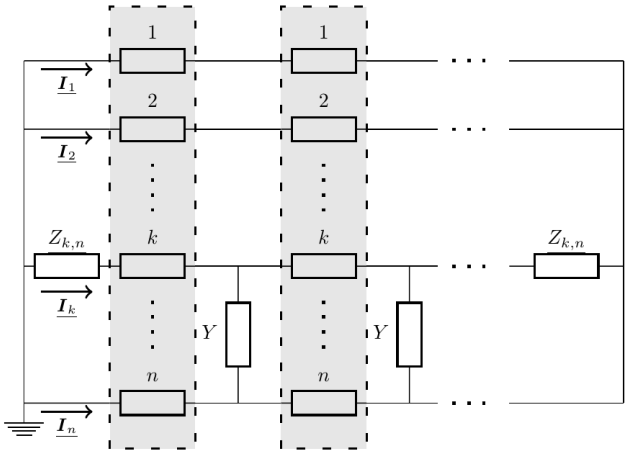

Figure 1: Scheme of the equivalent network embodying the characteristic matrices.

3. Results and Discussion

In order to highlight some of the key features of the presented methodology, two physical configurations of practical interest are evaluated. The former consists of a parallel routing, where the pipeline's horizontal distance from the power line (h_d) remains constant for the whole zone of influence, whereas the latter presents a more involved geometry, including a crossing, studied for a range of different crossing angles. The two different configurations are sketched in Fig. 2. In both cases, the power line (Fig. 3)

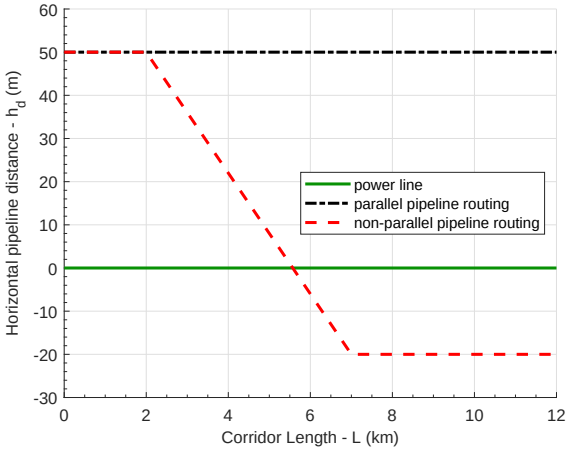

Figure 2: Sketch of the right-of-way for a parallel configuration and an oblique configuration with a crossing angle of $\alpha = 0.8021°$.

consists of three line conductors and two overhead ground wires (OGWs). In order to provide a reference point for the subsequent result analysis, the geometric and electrical

properties of the power line and the buried pipeline, the line currents and the soil are retained for both tests. This way, the observed behaviour in the induced voltages and currents can be fully attributed to the different routing (or to a different discretization process). The details regarding the considered materials and radii of the conductors are shown in Tab. 1, whereas their geometrical position is depicted in Fig. 3. The line conductors are numbered using arabic numbers, while roman numbers are employed to indicate the two OGWs.

Table 1: Geometrical and electrical data

Physical quantity	**Value**	**Unit Measure**
I_{l-1} (line conductor)	$750\angle 0^\circ$	A
I_{l-2} (line conductor)	$750\angle -120^\circ$	A
I_{l-3} (line conductor)	$750\angle 120^\circ$	A
σ_s (soil)	$2 \cdot 10^{-2}$	S/m
σ_p (pipeline)	$5 \cdot 10^{6}$	S/m
$radius_{ext}$ (pipeline)	0.4	m
$radius_{int}$ (pipeline)	0.375	m
μ_r (pipeline)	1	–
ρ_{coat} (pipeline coating)	$2.5 \cdot 10^{6}$	$\Omega \cdot$ m
ϵ_{coat} (pipeline coating)	5	–
σ_{line} (line conductor)	$5.9 \cdot 10^{7}$	S/m
$radius_{line}$ (line conductor)	$1.6 \cdot 10^{-2}$	m
σ_{ogw} (OGW)	$5.9 \cdot 10^{7}$	S/m
$radius_{ogw}$ (OGW)	$6 \cdot 10^{-3}$	m

3.1. Parallel routing

For this first test, an exposure length L of 12 km has been considered, with a constant horizontal distance $h_d = 50$ m of the pipeline from the centre of the power line. The pipeline is assumed to be earthed at both ends of its path, i.e., at 0 m and 12 km, with resistance 5 Ω. Also, the pipeline's non-ideal coating has been taken into account, and a per-unit-length value of admittance to earth $\underline{Y'} = 9.4 \cdot 10^{-4} + j3 \cdot 10^{-6}$ S/m has been considered for each cell of the equivalent circuit. This value of $\underline{Y'}$ is realistic for a 4 mm thick bituminous coating [4]. Since this configuration features a parallel pipeline-power line routing, a single characteristic matrix was employed. This has been obtained following the procedure described in Section 2, by gathering the currents induced in each conductor when the $i-$th one is subject to a unit value of $\underline{J_{z,0}}$ current density. As an example, Fig. 4 shows the computed distribution of magnetic vector potential in the soil when $\underline{J_{z,0}} = 1$ is enforced on OGW II (see Fig. 3 for reference). Once obtained the characteristic matrix by means of the finite element analysis, the total length of the corridor L has been covered by concatenating 500 cells of length $L_{cell} = 50$ m each. This allows to adequately the transversal currents flowing through the imperfect coating (represented by the admittance Y of Fig. 1) The computed longitudinal current and pipeline-to-earth voltage are plotted in Fig. 5.

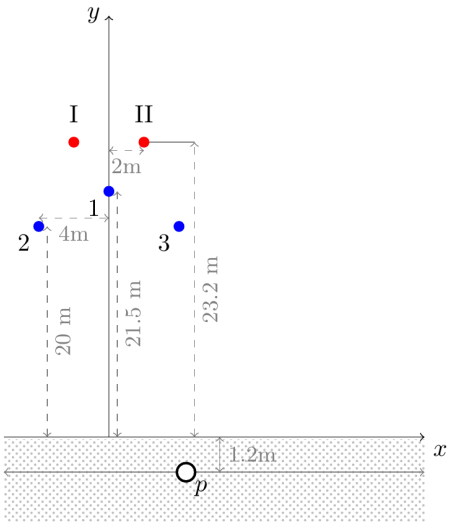

Figure 3: Geometrical positions of the conductors.

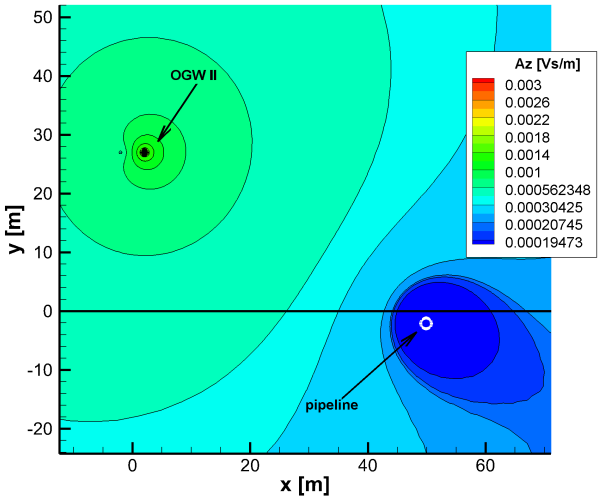

Figure 4: Distribution of $|\underline{A_z}|$ when $\underline{J_{z,0}} = 1$ on OGW II, with $h_d = 50\,\mathrm{m}$.

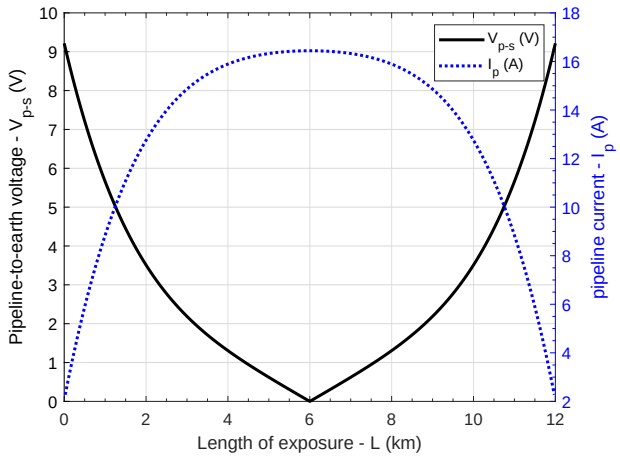

Figure 5: Numerical results for the parallel routing.

The obtained profiles are compatible with the results yielded by the classic circuital methodologies [4, 19]. The low values of longitudinal current I_p at both ends of the exposure length are due to the pipeline earthings. Dually, the induced voltage to earth - obtained as the voltage drop over the ith admittance to earth - reaches its minimum at $L/2$. The reason behind this is that the computed voltage to earth is proportional to the current flowing through the coating, which is in turn determined by the difference between the longitudinal pipeline currents belonging to the ith and $(i+1)$th cell of the equivalent electrical circuit.

3.2. Nonparallel routing and convergence analysis

As anticipated, a second test has been conducted, retaining all the physical and geometrical parameters of the previous one but changing the routing of the pipeline with respect to the power line. In particular, the pipeline is assumed to cross over the power line at $L = 5571\,\mathrm{m}$.

This raises the issue of how a nonparallel path should be discretized. As already mentioned, the basic idea for discretizing a nonparallel path is to represent the crossing as a certain number of parallel segments, forming a broken line; however, the number of segments to be employed - which corresponds to the number of computed characteristic matrices - can influence the accuracy of the calculations. For this reason, the routing described in Fig. 2 has been discretized in four different ways (which will be referred from here onward as Case I, Case II, Case III and Case IV), by progressively increasing the number of employed characteristic matrices (hence discretized sections of the geometry). Subdividing the routing in n sections implies computing n meshes, in which the horizontal distance of the pipeline from the power line centre h_d is progressively varied according to the right-of-way being sampled. Then, for each computed mesh, the characteristic matrix is extracted following the procedure described in Section 2, and used to perform the circuital analysis. The four longitudinal discretizations adopted in Cases I-IV, along with the obtained profiles of voltage-to-earth and current of the pipeline are

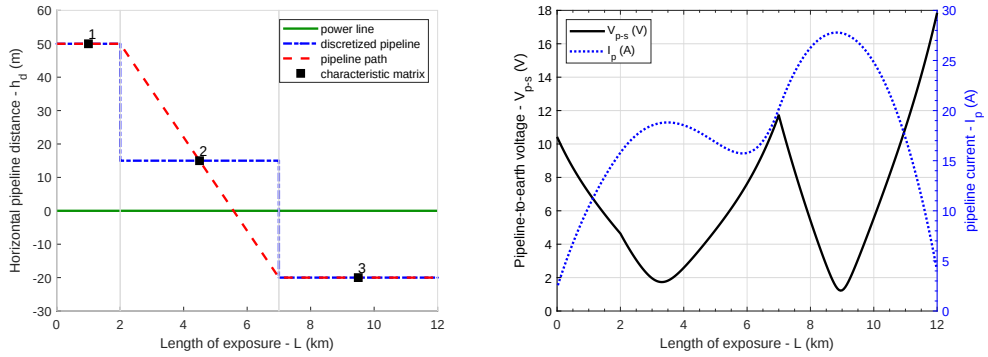

(a) (b)

Figure 6: CASE I - Routing discretization employing 3 characteristic matrices(a) and resulting induced voltage and current on the pipeline (b).

represented in Fig. 6 to Fig. 9. The right-of-way has been discretized using 3, 6, 11 and 17 sections, respectively, each represented by its characteristic matrix, corresponding to a different value of h_d. In the network analysis, the i-th characteristic matrix is associated with a certain length, eventually summing up to the total length of exposure L. The length associated to each characteristic matrix can be inferred from the blue, dashed line indicated as "discretized pipeline" in Fig. 6a to Fig. 9a. As one can see by looking at the evolution of the obtained voltage and current profiles, the four different numbers of employed characteristic matrices yield different physical results, both in terms of the shape and the magnitude of the induced electromagnetic variables. The four different voltage-to-earth profiles are plotted comparatively in Fig. 10. As expected, the relative differences between the obtained solutions decrease when more characteristic matrices are employed. This allows us to presume that further discretization refinement would not produce any significant improvement in the solution accuracy. Keeping in mind that the oblique section only is being discretized differently, one can see that – with the exception of Case I – the other profiles are almost coincident at both ends of the considered corridor. In other words, even the coarse subdivision employed in Case II appears to be sufficient if the oblique part of the path is not of particular technical concern. Nevertheless, focusing on the oblique part of the pipeline path, the choice of Case II over Case IV would approximately lead to an 8% overestimation of the maximum induced voltage magnitude. This could have relevant technical implications, as the technical standards prescribe the adoption of mitigation measures upon reaching specific values of induced voltage-to-earth of the pipeline.

Comparing the obtained profiles of longitudinal current and pipeline-to-earth voltage with the ones of Fig. 5 (relative to a parallel routing), it is evident that a variation of the pipeline positioning with respect to the interference source can significantly alter the magnitude and profile of the induced voltages and currents. Comparing the results of Fig. 5 and Fig. 9b, the nonparallel routing is responsible for an increase of the maximum magnitudes of both the induced voltage and current on the pipeline by a factor 3 and 1.76, respectively.

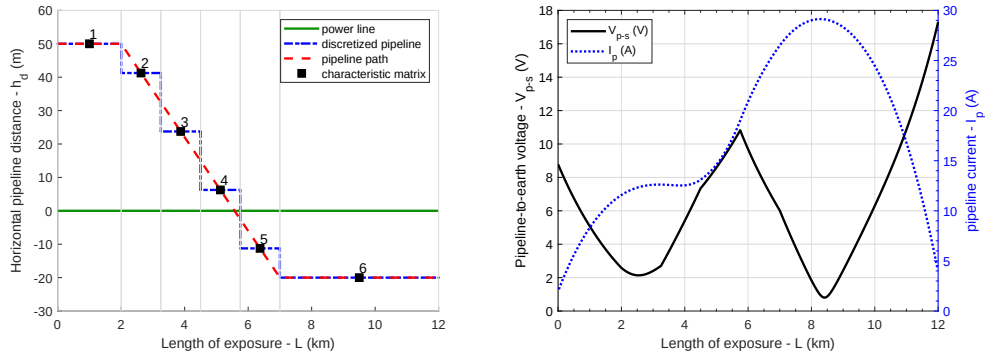

(a) (b)

Figure 7: CASE II - Routing discretization employing 6 characteristic matrices (a) and resulting induced voltage and current on the pipeline (b).

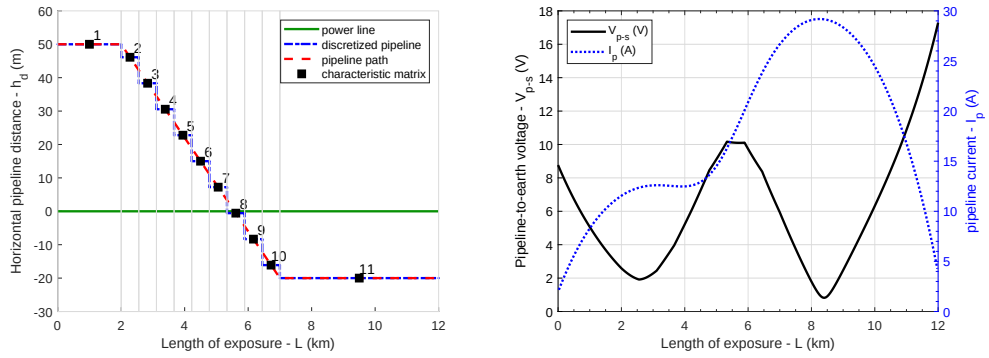

(a) (b)

Figure 8: CASE III - Routing discretization employing 11 characteristic matrices (a) and resulting induced voltage and current on the pipeline (b).

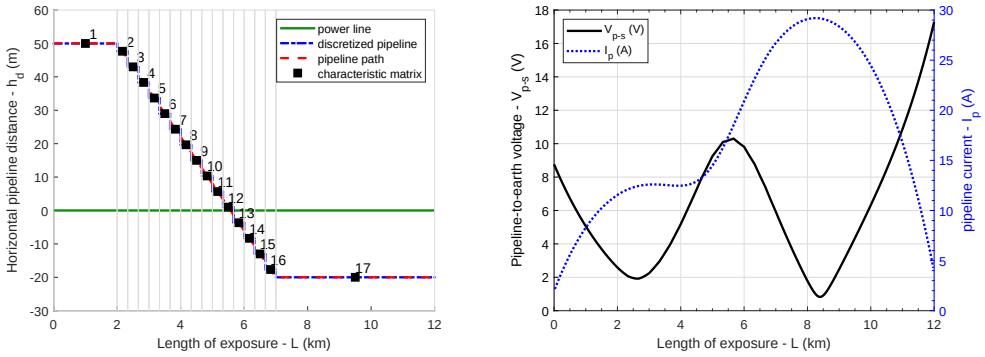

(a) (b)

Figure 9: CASE IV - Routing discretization employing 17 characteristic matrices (a) and resulting induced voltage and current on the pipeline (b).

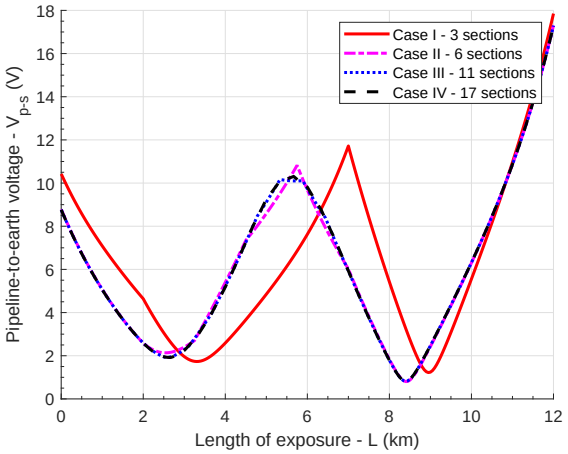

Figure 10: Comparison between the different voltage profiles yielded by the four considered routing discretizations (convergence test).

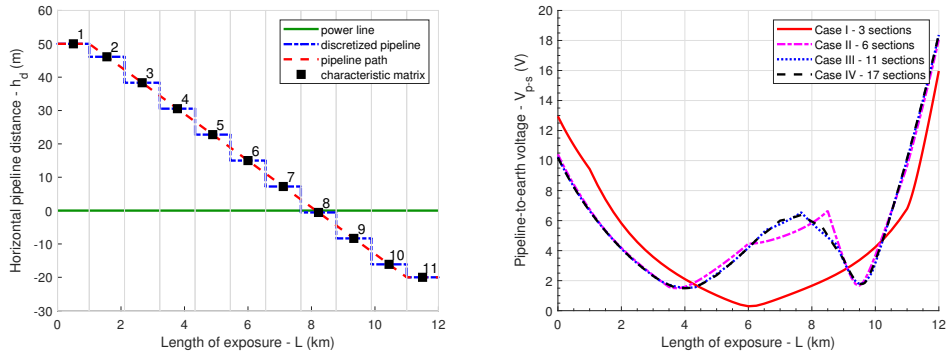

(a) (b)

Figure 11: Routing for a crossing angle of 0.5α (a) and convergence test for a crossing angle of 0.5α (b).

Finally, it is also worth stressing out that - despite having largely employed network analysis throughout this work - the obtained results should not be considered as the output of a circuital analysis of the physical problem. Indeed, as stated in Section 2, the network analysis is just a tool to enforce some constraints on the results yielded by the 2D FEM analysis, such as the soil acting as a return path for the pipeline and the OGWs, or the pipeline's earthings and non ideal coating. As a consequence of that, the results produced by the network analysis for every cell of the equivalent circuit can be re-introduced in the FEM code as forcing terms. In such way, the 2D FEM will yield results that are consistent with the constraints enforced via the network analysis, and thus allow the detailed knowledge of the electromagnetic fields distribution in every section of the considered right-of-way.

3.3. Influence of the crossing angle

The results presented in the previous section have been obtained assuming a crossing angle $\alpha = 0.8021°$. The angle α results from a 70 m displacement of the horizontal distance of the pipeline with respect to the power line centre h_d, over a longitudinal length of 5 km. In this section, the calculations are repeated for a range of crossing angles. Firstly, the convergence test described in Section 3.2 has been performed for angles of 0.5α and 2α. The obtained results are reported in Fig. 11 (0.5α) and Fig. 12 (2α). The comparison of the convergence tests performed for 0.5α and 2α, together with the already discussed crossing angle α, suggests a trend in the results: the accuracy of the oblique path discretization becomes less important as the crossing angle increases. In Fig. 11b, a sharp change can be noticed between the pipeline-to-earth voltages obtained using 6 and 11 sections (hence characteristic matrices). Conversely, the same two voltages in Fig. 12b appear to be significantly closer one to another. Provided that inductive coupling cannot take place between two perpendicular infinite conductors [4, 5], the obtained results are explained by noticing that the adoption of a higher crossing angle implies reducing the longitudinal "active" distance covered by the oblique part of the pipeline path. This holds if the horizontal distances h_d of the initial and final parallel sections of the routing are kept constant. This, in turn, reduces the overall electromagnetic contribution given by

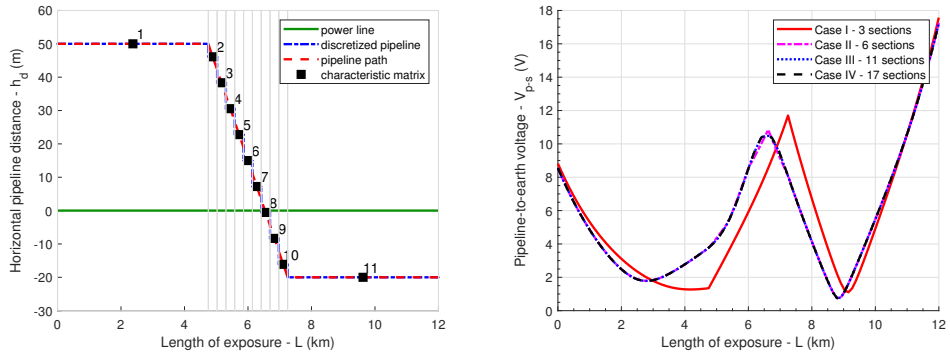

(a) (b)

Figure 12: Routing for a crossing angle of 2α (a) and convergence test for a crossing angle of 2α (b).

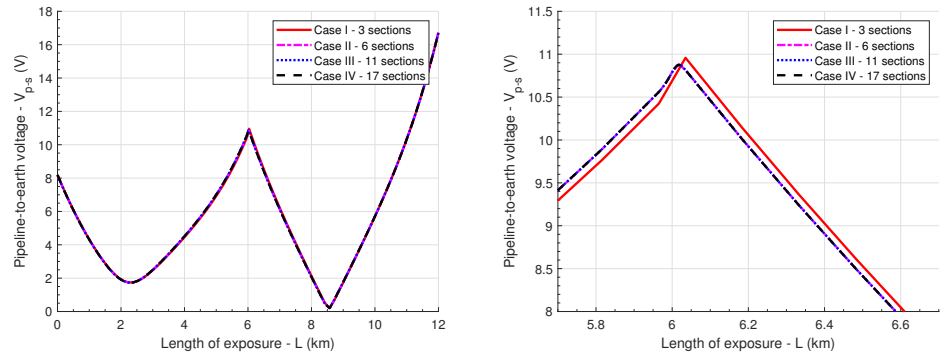

(a) (b)

Figure 13: Routing for a crossing angle of 45° (a) and convergence test for a crossing angle of 45° (b).

the oblique part of the pipeline path to the induced voltage profile over the whole corridor length. Furthermore, the convergence tests have also been repeated assuming 30°, 45° and 60° for the oblique path. The results obtained for a convergence test performed for a 45° crossing can be observed in 13a. However, as one can see, the different discretization processes yield very similar voltage profiles for this angle. A detail in proximity of the length at which the crossing occurs is shown in Fig. 13b. As previously mentioned, the adoption of larger crossing angles with respect to Fig. 11 and Fig. 12 has the effect of reducing the electromagnetic contribution (in terms of both induced voltages and currents) of the oblique part of the pipeline path; that is, the solution is dominated by the parallel parts of the right-of-way, while the oblique part (and hence its discretization) does not affect significantly the solution. The convergence test shown in Fig. 13a is not reported for the 30° and 60° crossings, as the results are very similar to the 45° case for the above reasons.

Finally, Fig. 14 shows the computed pipeline-to-earth voltage and pipeline current

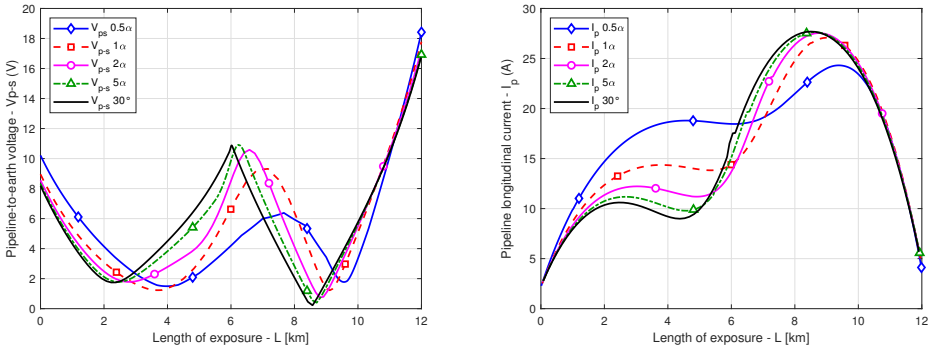

(a) (b)

Figure 14: Voltage (a) and current (b) induced on a pipeline crossing a straight power line for several angles from 0.5α to 30°.

for all considered crossing angles up to 30°. The 45° and 60° results have been omitted for the sake of conciseness. Also, an additional crossing angle equal to 5α has been added to highlight the progressive transition of the obtained results. The voltage and current profiles shown in Fig. 14 have been obtained using 17 characteristic matrices. It is interesting to notice that, once past an angle of 5α, the results show only small changes when the crossing angle is increased. This is compatible with the results shown in the previous results for 0.5α, α, 2α and 45°, and with the available technical literature. Indeed, the CIGRE technical guide devoted to the influence of high voltage A.C. power systems on metallic pipelines states that "if the acute angle between line and pipeline is larger than 45°, the section can be neglected" [4].

4. Conclusions

In this paper, a quasi-3D approach has been applied to analyse two different cases of interference caused by the vicinity of a metallic pipeline, buried in the soil, to a transmission line. The first case consists of a pipeline running parallel to a power line, whereas the second involves an intersection between the paths of the two structures. Four different discretizations of the routing have been investigated, by comparing the differences in the computed induced voltage profiles. Afterwards, a set of different crossing angles has been assessed and discussed. Similar trends for the induced currents and voltages obtained for the simple parallel routing can be found in literature, yielded by circuital and analytical methodologies, such as [4]. This shows that the proposed approach is valid and applicable to realistic (and intricate) physical configurations , such as the crossing considered in Section 3.2. Indeed, the proposed methodology can be successfully employed in presence of arbitrarily complex electrical properties of the soil [17], and with any number of metallic objects such as mitigation wires buried alongside the pipeline [20]. Finally the results obtained for different crossing angles indicate that, whenever an oblique path is dicretized with a set of parallel segments, a convergence analysis should be performed

to ensure that the discretization process does not affect the obtained results, especially when small crossing angles are considered.

References

[1] G. Lucca, Different approaches in calculating ac inductive interference from power lines on pipelines, IET Science, Measurement Technology 12 (2018) 802–806. doi:10.1049/iet-smt.2018.0086.

[2] A. Taflove, J. Dabkowski, Prediction Method for Buried Pipeline Voltages Due to 60 Hz AC Inductive Coupling Part I-Analysis, IEEE Transactions on Power Apparatus and Systems PAS-98 (1979) 780–787. doi:10.1109/TPAS.1979.319290.

[3] J. Dabkowski, A. Taflove, Prediction Method for Buried Pipeline Voltages Due to 60 Hz AC Inductive Coupling Part II–Field test Verification, IEEE Transactions on Power Apparatus and Systems PAS-98 (1979) 788–794. doi:10.1109/TPAS.1979.319291.

[4] CIGRE, Guide on the Influence of High Voltage AC Power Systems on Metallic Pipelines, Technical Report, Cigré Working Group 36.02, 1995.

[5] ITU-T, CCITT Directives Volume III: Calculating induced voltages and currents in pratical cases, Technical Report, ITU-T, 1989.

[6] A. Cristofolini, A. Popoli, L. Sandrolini, A comparison between Carson's formulae and a 2D FEM approach for the evaluation of AC interference caused by overhead power lines on buried metallic pipelines, Progress In Electromagnetics Research C 79 (2017) 39–48.

[7] G. C. Christoforidis, D. P. Labridis, P. S. Dokopoulos, A hybrid method for calculating the inductive interference caused by faulted power lines to nearby buried pipelines, IEEE Transactions on Power Delivery 20 (2005) 1465–1473. doi:10.1109/TPWRD.2004.839186.

[8] A. Popoli, L. Sandrolini, A. Cristofolini, Finite element analysis of mitigation measures for ac interference on buried pipelines, in: 2019 IEEE International Conference on Environment and Electrical Engineering and 2019 IEEE Industrial and Commercial Power Systems Europe (EEEIC / I CPS Europe), 2019, pp. 1–5. doi:10.1109/EEEIC.2019.8783843.

[9] H. Tiegna, Y. Amara, G. Barakat, Overview of analytical models of permanent magnet electrical machines for analysis and design purposes, Mathematics and Computers in Simulation 90 (2013) 162 – 177. doi:https://doi.org/10.1016/j.matcom.2012.12.002, eLECTRIMACS 2011- PART I.

[10] N. M'ziou, Electromagnetic compatibility problems of indirect lightning stroke on overhead power lines, Mathematics and Computers in Simulation (2018). doi:https://doi.org/10.1016/j.matcom.2018.04.007.

[11] D. D. Micu, G. C. Christoforidis, L. Czumbil, AC interference on pipelines due to double circuit power lines: A detailed study, Electric Power Systems Research 103 (2013) 1 – 8. doi:http://dx.doi.org/10.1016/j.epsr.2013.04.008.

[12] F. P. Dawalibi, R. D. Southey, Analysis of electrical interference from power lines to gas pipelines. I. Computation methods, IEEE Transactions on Power Delivery 4 (1989) 1840–1846. doi:10.1109/61.32680.

[13] C. A. Charalambous, A. Demetriou, A. L. Lazari, A. I. Nikolaidis, Effects of electromagnetic interference on underground pipelines caused by the operation of high voltage ac traction systems: The impact of harmonics, IEEE Transactions on Power Delivery 33 (2018) 2664–2672. doi:10.1109/TPWRD.2018.2803080.

[14] N. Ida, Y. Le Menach, X. Shan, J. Payer, A nonlinear model for AC induced corrosion, Advanced Electromagnetics 1 (2012) 92–96. doi:10.7716/aem.v1i1.54.

[15] H. W. Liu, S. P. Zhan, Y. H. Du, P. Zhang, Study on pulsed eddy current nondestructive testing technology for pipeline corrosion defects based on finite element method, in: Applied Mechanics and Materials, volume 120, Trans Tech Publ, 2012, pp. 36–41.

[16] C. Munteanu, V. Topa, G. Mates, M. Purcar, A. Racasan, I. T. Pop, Analysis of the electromagnetic interferences between overhead power lines and buried pipelines, in: International Symposium on Electromagnetic Compatibility - EMC EUROPE, 2012, pp. 1–6. doi:10.1109/EMCEurope.2012.6396746.

[17] A. Popoli, L. Sandrolini, A. Cristofolini, A quasi-3D approach for the assessment of induced AC interference on buried metallic pipelines, International Journal of Electrical Power & Energy Systems 106 (2019) 538 – 545. doi:https://doi.org/10.1016/j.ijepes.2018.10.033.

[18] C. W. Steele, Numerical computation of electric and magnetic fields, Springer Science & Business Media, 2012.

[19] N. Tleis, Power Systems Modelling and Fault Analysis, Elsevier Ltd., 2008.

[20] A. Cristofolini, A. Popoli, L. Sandrolini, Numerical modelling of interference from ac power lines on buried metallic pipelines in presence of mitigation wires, in: Proc. 2018 IEEE International Conference on Environment and Electrical Engineering and 2018 IEEE Industrial and Commercial Power Systems Europe (EEEIC/I&CPS Europe), IEEE, 2018, pp. 1–6.